



Projected near-term changes in three types of heat waves over China under RCP4.5

Qin Su¹ · Buwen Dong²

Received: 21 September 2018 / Accepted: 21 March 2019 / Published online: 2 April 2019
© Springer-Verlag GmbH Germany, part of Springer Nature 2019

Abstract

The changes in three aspects of frequency, intensity and duration of the compound, daytime and nighttime heat waves (HWs) over China during extended summer (May–September) in a future period of the mid-21st century (FP; 2045–2055) under RCP4.5 scenario relative to present day (PD; 1994–2011) are investigated by two models, MetUM-GOML1 and MetUM-GOML2, which comprise the atmospheric components of two state-of-the-art climate models coupled to a multi-level mixed-layer ocean model. The results show that in the mid-21st century all three types of HWs in China will occur more frequently with strengthened intensity and elongated duration relative to the PD. The compound HWs will change most dramatically, with the frequency in the FP being 4–5 times that in the PD, and the intensity and duration doubling those in the PD. The changes in daytime and nighttime HWs are also remarkable, with the changes of nighttime HWs larger than those of daytime HWs. The future changes of the three types of HWs in China in two models are similar in terms of spatial patterns and area-averaged quantities, indicating these projected changes of HWs over the China under RCP4.5 scenario are robust. Further analyses suggest that projected future changes in HWs over China are determined mainly by the increase in seasonal mean surface air temperatures with change in temperature variability playing a minor role. The seasonal mean temperature increase is due to the increase in surface downward longwave radiation and surface shortwave radiation. The increase in downward longwave radiation results from the enhanced greenhouse effect and increased water vapour in the atmosphere. The increase in surface shortwave radiation is the result of the decreased aerosol emissions, via direct aerosol–radiation interaction and indirect aerosol–cloud interaction over southeastern and northeastern China, and the reduced cloud cover related to a decrease in relative humidity.

Keywords Heat wave · Heat wave type · Future change · China · Coupled models

1 Introduction

Heat waves (HWs) are usually defined as abnormally hot weather lasting for several days (Perkins and Alexander 2013; Perkins 2015). This distinct type of extreme temperature events has resulted in substantial socioeconomic loss

and risks to human health (e.g. Robine et al. 2008; Coumou and Rahmstorf 2012; Hatfield and Prueger 2015; Lesk et al. 2016). Over the last two decades, HWs have occurred more frequently all over the world (e.g., Meehl and Tebaldi 2004; Seneviratne et al. 2014). Without any exception, several severe HWs hit China recently in different regions and broke the regional historical temperature records, such as the 2013 July–August HW in the lower reaches of the Yangtze River Valley (Sun et al. 2014; Zhou et al. 2014b; Ma et al. 2017), the 2015 summer HW in western China (Sun et al. 2016) and the 2017 July HW in central-eastern China (Chen et al. 2019; Sparrow et al. 2018). These catastrophic events led to enormous economic loss and heat-related morbidity and mortality (e.g., Tan et al. 2007; Sun et al. 2016; Ma et al. 2017). The increased occurrence of HWs largely results from the increased mean temperature (Argueso et al. 2016; Su and Dong 2019). The global warming is accelerated

Electronic supplementary material The online version of this article (<https://doi.org/10.1007/s00382-019-04743-y>) contains supplementary material, which is available to authorized users.

✉ Qin Su
suqin@ynu.edu.cn

¹ Department of Atmospheric Sciences, Yunnan University, Kunming 650091, China

² Department of Meteorology, National Centre for Atmospheric Science-Climate, University of Reading, Reading, UK

and the warming at 2 °C above pre-industrial levels will occur around 2045, much earlier than that in the special report of Intergovernmental Panel on Climate Change (Xu et al. 2018). With the rapid increase in mean temperatures, the projection of HWs in the near term, such as mid-21st century, should be paid more attention to and would be an important issue for developing climate adaptation strategies.

A HW could take place on daytime, nighttime, or both. With different timing of occurrence, the HWs are related to different mechanisms and have different impacts (Gershunov et al. 2009; Freychet et al. 2017). The HWs in the day, usually associated with dry conditions (Black et al. 2004; Gershunov et al. 2009; Wang et al. 2016), have a variety of disastrous impacts on infrastructures, ecosystem, and human life (Wilbanks and Fernandez 2014), while the HWs at night, related to wet conditions (Gershunov et al. 2009; Chen and Lu 2014), have relatively weak impact. However, with the hot nights enhancing the damages of daytime high temperatures on human health (Gosling et al. 2009), the HWs persisting throughout the day and night are the most disastrous among these three types of HWs (Karl and Knight 1997). Thus, recent studies applied a more precise classification of HWs according to the timing of their occurrence to get more insights, which divided the HWs into three types, i.e., daytime, nighttime and compound ones (e.g., Chen and Li 2017; Chen and Zhai 2017; Freychet et al. 2017; Su and Dong 2019).

In recent decades since the mid-20th century, the previously-defined HWs, which only consider the daytime temperatures and involve the daytime HWs and part of the compound HWs, show increasing frequency and duration over China (Li et al. 2017; Luo and Lau 2017; Wang et al. 2017; You et al. 2017). Some recent studies, investigating the precisely defined daytime, nighttime and compound HWs over most of China, show significant increasing trends in frequency, intensity, and duration of them (Chen and Zhai 2017; Freychet et al. 2017). Notably, the increase in frequency and intensity of compound and nighttime HWs is much greater than that for daytime ones (Chen and Li 2017; Chen and Zhai 2017; Su and Dong 2019). Anthropogenic influences are highlighted to play crucial roles in the sharp increase in HW occurrence over China (e.g., Wilcox et al. 2015; Freychet et al. 2018).

Considering the anthropogenic influences, future changes in the HWs and temperature extremes over China are assessed under different scenarios. There would be an increase in warm extremes and a decrease in cold extremes under a warming climate (Zhou et al. 2014a; Yu et al. 2018). The frequency and duration of previously-defined HWs over China would increase and the increase would become larger when the mean temperature gets greater (Guo et al. 2017). However, only the future changes in previously-defined HWs are estimated and the assessment of future changes in

precisely defined compound, daytime, and nighttime HWs is still lacking. Furthermore, the projections outlined above are from fully coupled general circulation models, which, however, exhibit significant biases in simulated sea surface temperature that challenge the reliability of climate projections (Wang et al. 2014).

Therefore, the main aims of this work are to estimate the future changes in the daytime, nighttime, and compound HWs over China and to reveal the associated physical processes by using two near-globally coupled models comprising the atmospheric components of two state-of-the-art climate models coupled to a multi-level mixed-layer ocean and having a much smaller bias in simulated sea surface temperature (Hirons et al. 2015; Dong et al. 2017; Luo et al. 2018). The structure of this paper is organized as follows. The model and experiments are described in Sect. 2. Model simulated extended seasonal mean surface air temperatures and definition of HWs are described in Sect. 3. The projected changes in the three types of HWs are shown in Sect. 4. The physical processes responsible for future changes in HWs are illustrated in Sect. 5. Finally, the conclusions are summarized in Sect. 6.

2 Models and experiments

2.1 Models

Two coupled models, MetUM-GOML1 and MetUM-GOML2 (Hirons et al. 2015), which comprise the atmospheric components of two state-of-the-art climate models coupled to a multi-level mixed-layer ocean model, are used in this study. The atmospheric component for MetUM-GOML1 is the Met Office Unified Model (MetUM) at the fixed scientific configuration Global Atmosphere 3.0 (GA3.0; Arribas et al. 2011; Walters et al. 2011). The atmospheric component for MetUM-GOML2 is the MetUM GA6.0. The most notable change in GA6.0 compared with GA3.0 is that the “New Dynamics” dynamical core is replaced with “ENDGame” (Walters et al. 2014). ENDGame maintains the benefits of “New Dynamics”, whilst improving its accuracy, stability and scalability. The improved accuracy significantly reduces the model’s implicit damping, leading to an improvement to various modes of variability, such as the vertical height of extra-tropical cyclones and the structure of frontal systems. A detailed description of GA6.0 is given by Walters et al. (2017). The resolution for these two atmospheric models is 1.875° longitude by 1.25° latitude with 85 vertical layers. The models include an interactive tropospheric aerosol scheme, that is able to simulate the direct, indirect and semi-direct effects of aerosols (Jones et al. 2011; Walters et al. 2011). The oceanic components for MetUM-GOML1 and MetUM-GOML2 are the same,

which is a multi-column K profile parameterization (MC-KPP) mixed-layer ocean model. The horizontal resolution of MC-KPP is the same as that of the MetUM where it is coupled. The vertical resolution of MC-KPP is very high at the surface (1.2 m) and near the surface (2 m over the first 41.5 m), since the MC-KPP columns with 100 levels over a depth of 1000 m are defined using a stretch function. MC-KPP simulates only vertical mixing and does not include ocean dynamics, so corrections for temperature and salinity based on the seasonally-varying three-dimensional temperature and salinity flux are prescribed to represent the mean ocean advection and account for biases in atmospheric surface heat and fresh water fluxes. The atmospheric and oceanic components are coupled every 3 h. The air-sea coupling is limited by the maximum extent of a seasonally varying sea ice climatology (Hirons et al. 2015). These models are computationally cheaper than models with a fully interactive ocean. More importantly, they have a smaller bias in simulated sea surface temperature (Hirons et al. 2015, Dong et al. 2017; Luo et al. 2018) in comparison with fully coupled models (e.g., Wang et al. 2014) whilst also retaining intra-seasonal variability and coupling between the atmosphere and the ocean.

2.2 Experiments

The experiments performed in this study are summarized in Table 1. A 12-year relaxation experiment (R0) for MetUM-GOML1 and MetUM-GOML2 was firstly performed in which the MC-KPP profiles of temperature and salinity were relaxed to a present day (PD; 1994–2011) ocean temperature and salinity climatology derived from the Met Office ocean analysis (Smith and Murphy 2007). The relaxation experiment used PD anthropogenic greenhouse gas (GHG) and anthropogenic aerosol (AA) forcings (Lamarque et al. 2010, 2011). The daily mean seasonal cycle of ocean temperature and salinity corrections from the coupled relaxation experiment were then imposed in free-running coupled experiments. Three other time-sliced experiments using both models were performed using different forcings: the C-EP experiment forced by the early period (EP; 1964–1981) mean GHG concentrations and

AA emissions, the C-PD experiment forced by the PD (1994–2011) mean GHG concentrations and AA emissions; and the C-FP experiment forced by the future period (FP; 2045–2055) mean GHG concentrations and AA emissions under the Representative Concentration Pathway (RCP) 4.5 scenario. The single RCP4.5 scenario is chosen for projection because the radiative forcings in the four scenarios of RCP2.6, RCP4.5, RCP6.0, and RCP8.5 do not differ significantly in the FP of the mid-21st century (Moss et al. 2010). Relative to PD means, FP mean GHG concentrations increase (CO_2 by 30%, CH_4 by 4.5% and N_2O by 10.4%) and the emission of sulphur dioxide, which is one of the most important aerosol species, decreases over Europe (by 74%), East Asia (by 79%) and North America (by 81%) but increases over the Indian sub-continent (Fig. 1). All experiments were run for 50 years and used the climatological PD sea ice extent from the Met Office Hadley Center Sea Ice and Sea Surface Temperature data set (HadISST; Rayner et al. 2003). The last 45 years of each experiment were used for analysis.

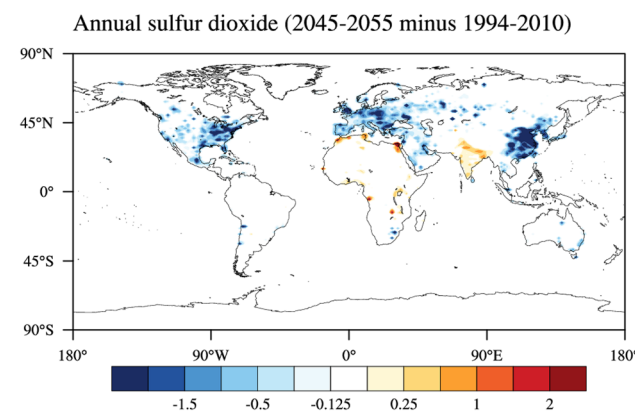


Fig. 1 Future changes in annual mean sulphur dioxide emissions (units: $\text{g m}^{-2} \text{year}^{-1}$) during the mid-21st century relative to the PD of 1994–2010

Table 1 Summary of numerical experiments

Abv.	Experiment	Ocean	Radiative forcing
R0	Relaxation run	Relaxation to “present day” (PD, 1994–2011) mean 3D ocean temperature and salinity to diagnose climatological temperature and salinity tendencies	PD greenhouse gases (GHGs) over 1994–2011 and anthropogenic aerosol (AA) emissions over 1994–2010 with AA after 2006 from RCP4.5 scenario (Lamarque et al. 2010, 2011)
C-EP	Early period (EP 1964–1981)	Climatological temperature and salinity tendencies	EP mean GHG and EP mean AA emissions
C-PD	Present day (PD 1994–2011)	from relaxation run	PD mean GHG and PD mean AA emissions
C-FP	Future period (FP, 2045–2055)		RCP4.5 emission scenario

3 Model-simulated seasonal mean surface air temperatures and heat waves during extended summer

3.1 Model performance in simulating early period surface air temperatures

The climatological means of daily maximum temperature (T_{\max}) and daily minimum temperature (T_{\min}) in the C-EP experiments of MetUM-GOML1 and MetUM-GOML2

for the extended summer are compared with the observed ones during EP (Fig. 2). The observational data used is the homogenized datasets of daily T_{\max} and T_{\min} series at 753 stations in China (Li et al. 2016). Observed T_{\max} pattern shows more or less uniform distributions over southeastern China with values higher than 28 °C and apparent meridional gradient over northeastern China. Over western China, a low-value centre is located over the Tibetan Plateau and a high-value centre over northwestern China with temperatures exceeding 28 °C (Fig. 2a). The observed climatological T_{\min} exhibits notable meridional gradient

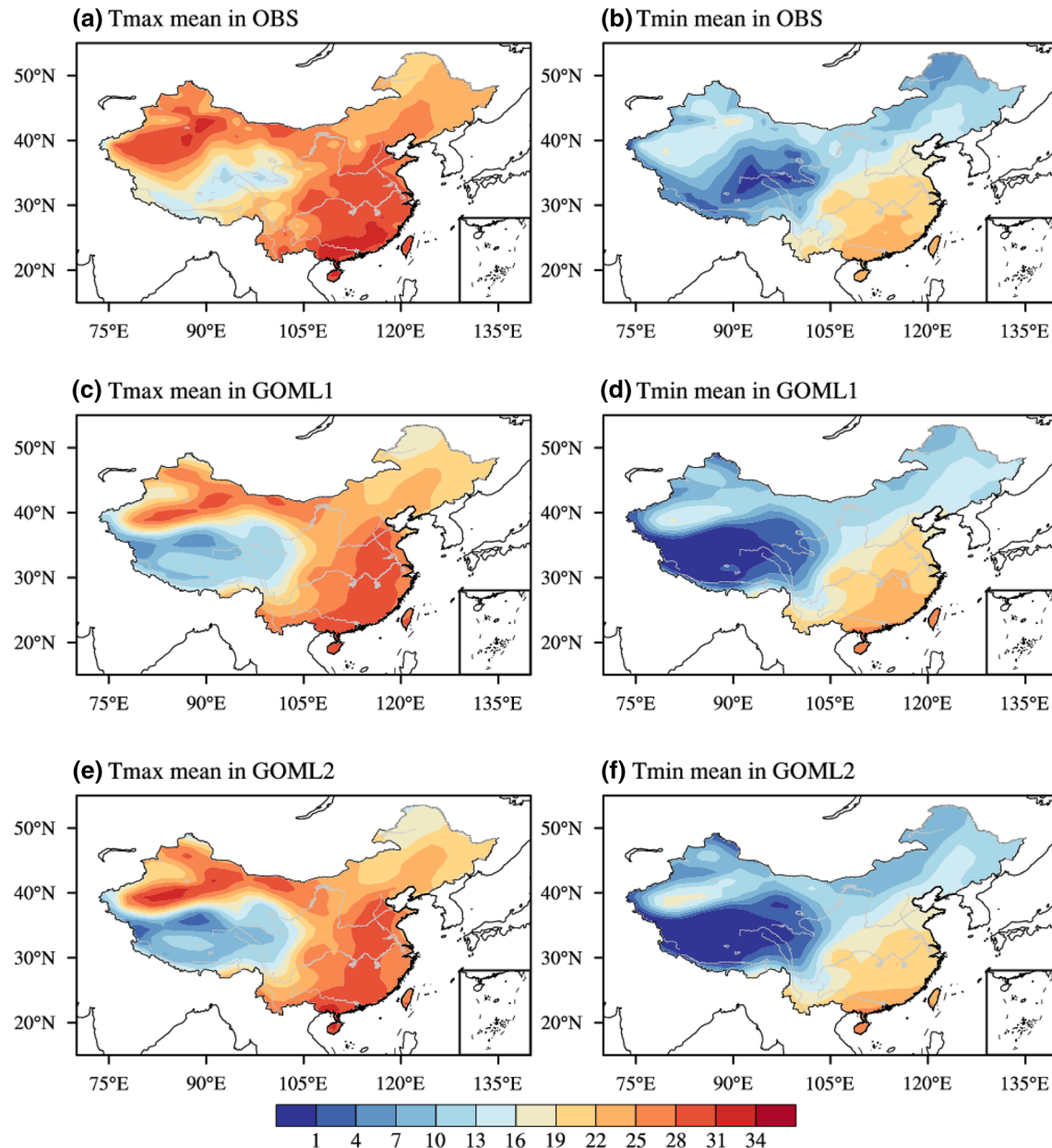


Fig. 2 Climatological means of extended-summer-mean (May–September) T_{\max} and T_{\min} during the EP (1964–1981) in observations (a, b) and in the C-EP experiment of MetUM-GOML1 (c, d) and MetUM-GOML2 (e, f). Units are in °C

over eastern China with the maximum higher than 22 °C at the southeast coast of China and minimum of 4–7 °C over northeastern China (Fig. 2b). The spatial distribution of T_{\min} over western China shows a minimum (less than 1 °C) over the Tibetan Plateau and a high value (more than 16 °C) over northwestern China, being similar to the spatial pattern in T_{\max} . The spatial patterns of climatological extended summer means of T_{\max} and T_{\min} and regional magnitudes in the C-EP experiments of both models agree well with the observations with pattern correlation coefficients of 0.85 and 0.86 for T_{\max} and 0.90 and 0.91 for T_{\min} , for MetUM-GOML1 and MetUM-GOML2, respectively (Fig. 2c–f). The two models reproduce the observed T_{\max} distributions over the southeastern and northwestern part of China with value above 28 °C, but slightly underestimate T_{\max} over the Tibetan Plateau and northeastern China (Fig. 2c, e). The distribution of observed T_{\min} is also well simulated by the model, despite some underestimation over the Tibetan Plateau (Fig. 2d).

3.2 Definition of heat waves

Three types of HWs, namely compound, daytime, and nighttime HWs, are defined in this study in the same way as the former study on decadal changes in HWs across the mid-1990s over China (Su and Dong 2019). Considering the various climate types in China, the relative threshold, which is determined by the local climate and varies at different places on different dates (Stefanon et al. 2012), is employed to define HWs over China in this study, following recent studies (e.g., Chen and Li 2017; Li et al. 2017; Wang et al. 2017). The relative threshold on each model calendar day is calculated as the daily 90th percentile of daily T_{\max} or T_{\min} based on 15-day samples centred on that day during the last 45 years of the C-EP experiment (i.e. total samples $15 \times 45 = 675$ days; Della-Marta et al. 2007). A compound HW, continuous hot weather in day and night, is defined when both T_{\max} and T_{\min} are higher than the thresholds for at least 3 days. A daytime (nighttime) HW, continuous hot weather only in the day (at night), is defined when only T_{\max} (T_{\min}) exceeds the thresholds for at least 3 days. The three types of HWs are independent of each other.

Three indicators, i.e. frequency, intensity and duration, are used to measure yearly HW activity. The frequency is represented by the accumulated occurrence of events in a given year. The intensity of each event is calculated by averaging the everyday temperature exceedance above the threshold within an event. Particularly, the intensity of compound HWs is the sum of the averaged T_{\max} and T_{\min} exceedances. The duration of each event is the number of days when an event endures. The intensity and duration for a given year is computed by averaging the intensity and duration of events occurring in that year.

3.3 Model performance in simulating early period heat waves

The frequency, intensity and duration of compound, daytime and nighttime HWs in the C-EP experiment of MetUM-GOML1 and MetUM-GOML2 during the extended summer are compared with those in observations in the EP (Fig. S1–3). In observations, the frequency, intensity and duration of compound HWs share similar spatial patterns, with relatively large values over southeastern China and the northern margin of mainland China (Fig. S1a–c). The daytime HWs in the EP are of the largest frequency and duration over western China and of the greatest intensity over the northern margin of mainland China (Fig. S2a–c). The frequency and duration of nighttime HWs are relatively high over central China and the intensity of nighttime HWs are the greatest over the northern margin of mainland China (Fig. S3a–c). The spatial patterns of the frequency, intensity and duration of all three types of HWs in observations are well reproduced by these two models, despite the underestimation of the frequency and duration of daytime HWs over western China. The biases of the area-averaged indices are examined by using the relative bias, which is defined as the absolute bias (model simulated index minus observational one) divided by observational index. The relative biases for various indices range from –12 to –43% in MetUM-GOML1 and –2 to –55% in MetUM-GOML2. According to Guo et al. (2017), which used 12 CMIP5 models to project the previously-defined HWs, the absolute value of the smallest relative bias of the previously-defined HWs in all 12 CMIP5 models is 36.66%. Comparing to their smallest relative bias, the smallest relative bias in MetUM-GOML1 and MetUM-GOML2 is much smaller, indicating a better ability of MetUM-GOML1 and MetUM-GOML2 in simulating the observed HWs. All the results above indicate these two models' capability of capturing the characteristics of the HWs in observations over China.

The good agreement in extended summer seasonal mean surface T_{\max} and T_{\min} between model simulations and observations and the models' ability of capturing the characteristics of the HWs over China suggest a fidelity of using these models for projecting their future changes. In addition, the C-EP and C-PD experiments were used to investigate the decadal changes in the East Asian summer monsoon, temperature extremes over China and HWs over China across the mid-1990s (Chen and Dong 2018; Su and Dong 2019; Tian et al. 2018). It is indicated by the previous studies that the circulation and precipitation over East Asia in present day and their decadal changes across the mid-1990s simulated by these two models are consistent with those in observations.

Previous studies of HWs over China demonstrated significant observed decadal changes in the frequency, intensity

and spatial pattern of the compound, daytime, and nighttime HWs across the mid-1990s (Chen and Li 2017; Chen and Zhai 2017; Su and Dong 2019). Su and Dong (2019) showed that the frequency of compound HWs averaged over China in the PD almost triples that in the EP while both intensity and spatial extent are almost doubled. Their analyses also indicated that the changes of daytime and nighttime HWs are also significant in all three aspects, though not as dramatical as those for compound HWs. They further attributed the observed decadal changes to changes in anthropogenic forcings.

In order to compare the projected future changes in context of model-simulated past decadal–multidecadal changes, the relative thresholds for three types of HWs in this study are based on early period C-EP simulations as described in above and used by Su and Dong (2019). Future changes in the HWs over China are indicated by the differences between the C-FP and C-PD experiments. Statistical significance of the mean changes was assessed using a two tailed Student's *t* test.

4 Future changes in heat waves over China

4.1 Spatial patterns of future changes

Figure 3 shows the projected future changes in compound HWs over China. The frequency, intensity and duration of compound HWs all increase significantly over China, but with different spatial patterns. The increase in frequency of compound HWs over the southern part of China is greater than that over the northern part. The southwest fringe of mainland China sees the greatest increase at more than 5.0 events per year (Fig. 3a, b). The intensity changes of compound HWs show much larger enhancement over the northern part of China than southern part (Fig. 3c, d). The duration of compound HWs over China increases with the largest change (more than 3.0 days) over southeastern China, western China and the southern part of northeastern China (Fig. 3e, f). Interestingly, the compound HWs over northern China and the Tibetan Plateau show the greatest relative changes in all frequency, intensity and duration (Fig. S4), but the frequency and duration of compound HWs over southern China are of much smaller relative changes though of the largest absolute changes (Fig. 3). Future changes of compound HWs in MetUM-GOML1 and MetUM-GOML2 are consistent with each other. However, there are some slight differences between them. For instance, the increase in frequency over northwestern China and the enhancement of intensity over northern China in MetUM-GOML2 (Fig. 3b, d) are slightly stronger than those in MetUM-GOML1 (Fig. 3a, c). Focusing on southern China, the increase in duration is greatest in southeastern China in

MetUM-GOML1 (Fig. 3e), compared with central-southern China in MetUM-GOML2 (Fig. 3f).

Future changes in daytime HWs are shown in Fig. 4. The frequency, intensity and duration of daytime HWs increase significantly over most of China. The frequency of daytime HWs increases most over the northwestern part of China and increases uniformly by 1.0–2.0 events per year over a large part of eastern China (Fig. 4a, b). The intensity of daytime HWs is enhanced more evenly than that of compound HWs with relatively strong enhancement of more than 0.6 °C/day over the southern part of China (Fig. 4c, d). The duration of daytime HWs are elongated over most of China, particularly with an increase of more than 2.0 days over the northwestern part of China (Fig. 4e, f). The ratios of the frequency, intensity and duration of daytime HWs in the FP to the PD (Fig. S5) share the similar spatial patterns with the absolute changes of them (Fig. 4). The future changes of daytime HWs are almost the same in the two models with very weak differences between them.

Future changes in nighttime HWs are illustrated in Fig. 5. Similar to compound and daytime HWs, all three features of nighttime HWs show significant increase over China. The spatial distributions of the increase in frequency and intensity of nighttime HWs are more uniform comparing to those of compound HWs. The increase in frequency of nighttime HWs is similar in magnitude over most of China, except for a relatively large increase over the southern margin of mainland China (more than 4.0 events per year; Fig. 5a, b). The increase in intensity of nighttime HWs is also largely uniform over most of China at 0.3–0.6 °C/day, though the northern margin of mainland China sees a greater enhancement of intensity (Fig. 5c, d). The duration of nighttime HWs extends longer relatively greatly over the Tibetan Plateau and the southeast coast of China with the largest changes of more than 3.0 days over the Tibetan Plateau (Fig. 5e, f). The patterns of relative changes of nighttime HWs (Fig. S6) are similar to those of the absolute changes (Fig. 5), except that the frequency over northeastern China and the intensity over the southern margin of mainland China show larger relative changes but smaller absolute changes, comparing to other regions. The spatial patterns of future changes in nighttime HWs in MetUM-GOML1 and MetUM-GOML2 are quite similar, despite some differences in intensity of changes, such as larger increases in frequency over the central-northern China and stronger enhancement of intensity over northern margin of mainland China in MetUM-GOML2 (Fig. 5b, d).

4.2 Area-averaged future changes

Figure 6 shows area-averaged future changes in frequency, intensity and duration of the three types of HWs over whole China and ratios of the FP projection to the PD value of

Compound HWs

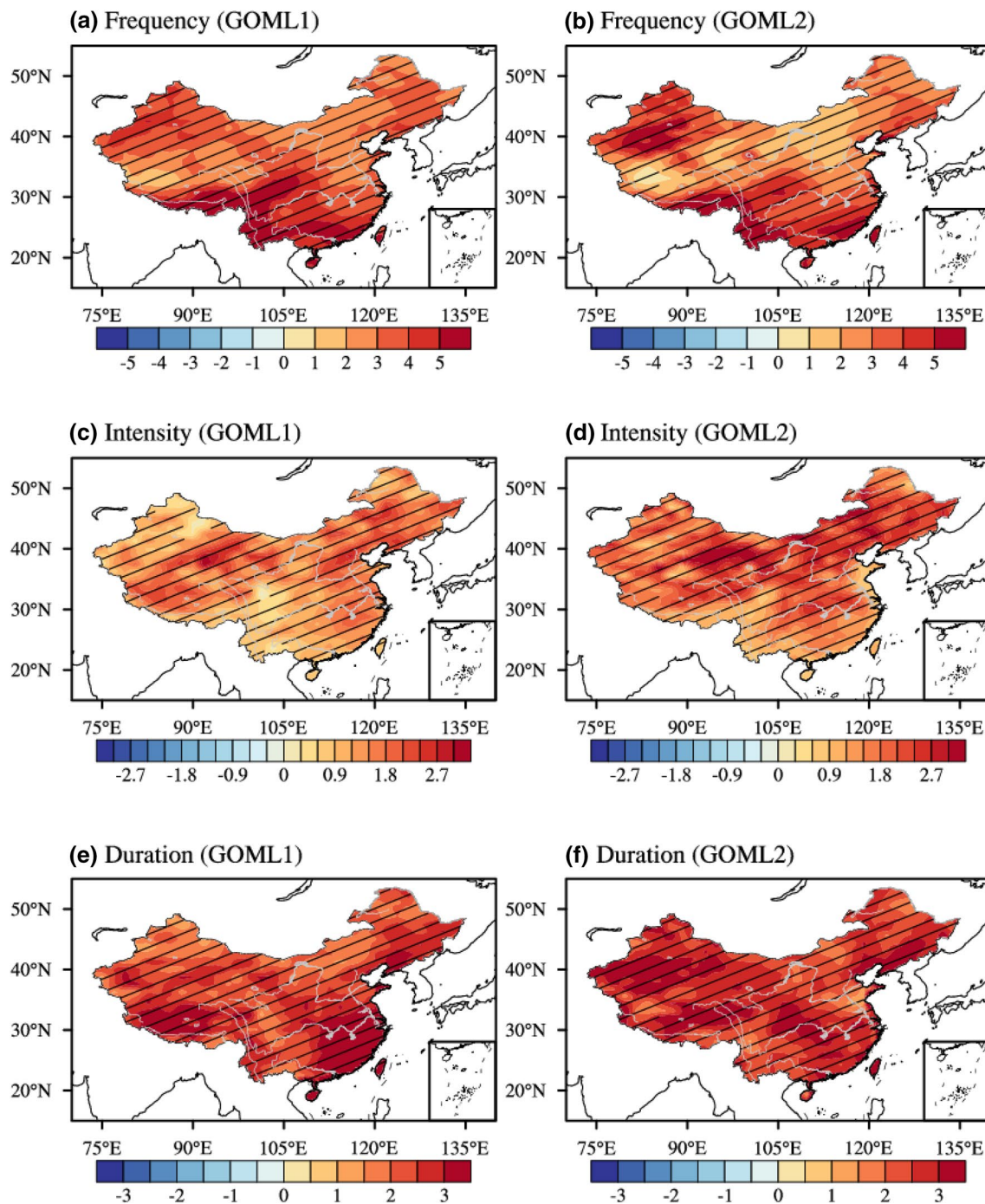


Fig. 3 Spatial patterns of future changes in frequency (units: events year⁻¹; **a, b**), intensity (units: °C day⁻¹; **c, d**), and duration (units: days; **e, f**) of compound HWs in MetUM-GOML1 (left panels) and MetUM-GOML2 (right panels), masked by China boundary.

The slashes highlight the regions where the differences are statistically significant at the 90% confidence level based on a two-tailed Student's *t* test

Daytime HWs

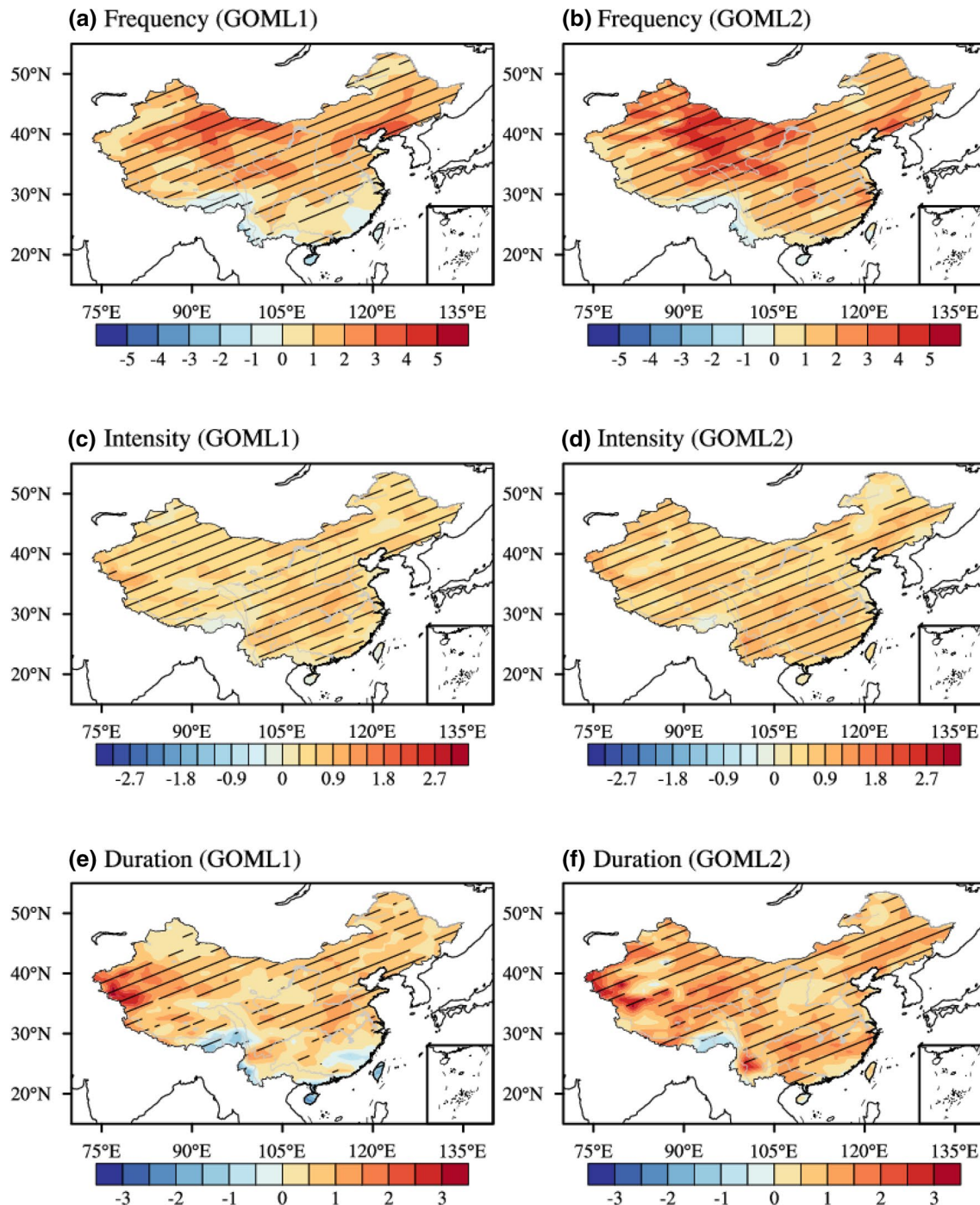


Fig. 4 Spatial patterns of future changes in frequency (units: events year⁻¹; **a, b**), intensity (units: °C day⁻¹; **c, d**), and duration (units: days; **e, f**) of daytime HWs in MetUM-GOML1 (left panels) and MetUM-GOML2 (right panels), masked by China boundary. The

slashes highlight the regions where the differences are statistically significant at the 90% confidence level based on a two-tailed Student's *t* test

Nighttime HWs

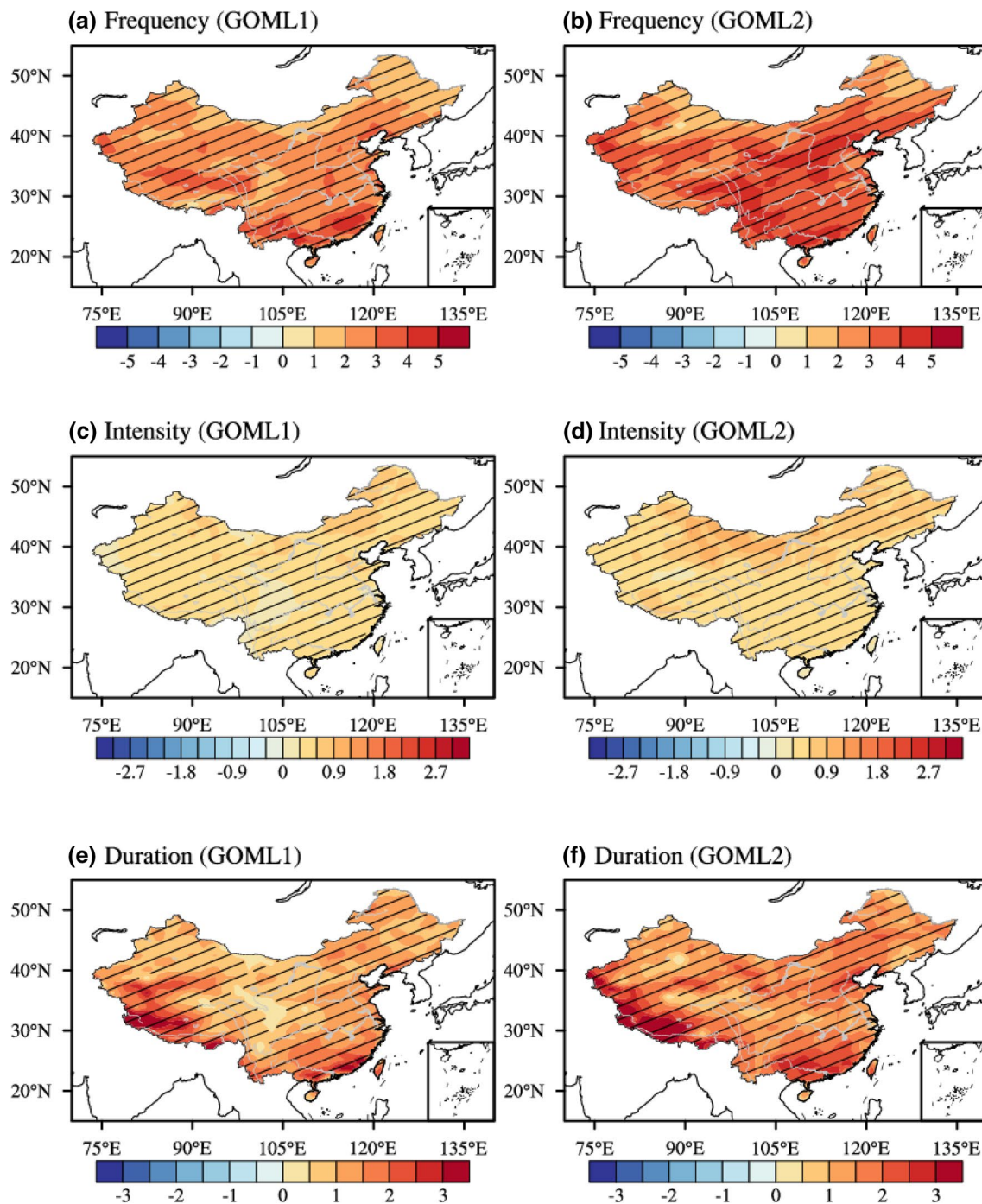


Fig. 5 Spatial patterns of future changes in frequency (units: events year⁻¹; **a, b**), intensity (units: °C day⁻¹; **c, d**), and duration (units: days; **e, f**) of nighttime HWs in MetUM-GOML1 (left panels) and MetUM-GOML2 (right panels), masked by China boundary. The

slashes highlight the regions where the differences are statistically significant at the 90% confidence level based on a two-tailed Student's *t* test

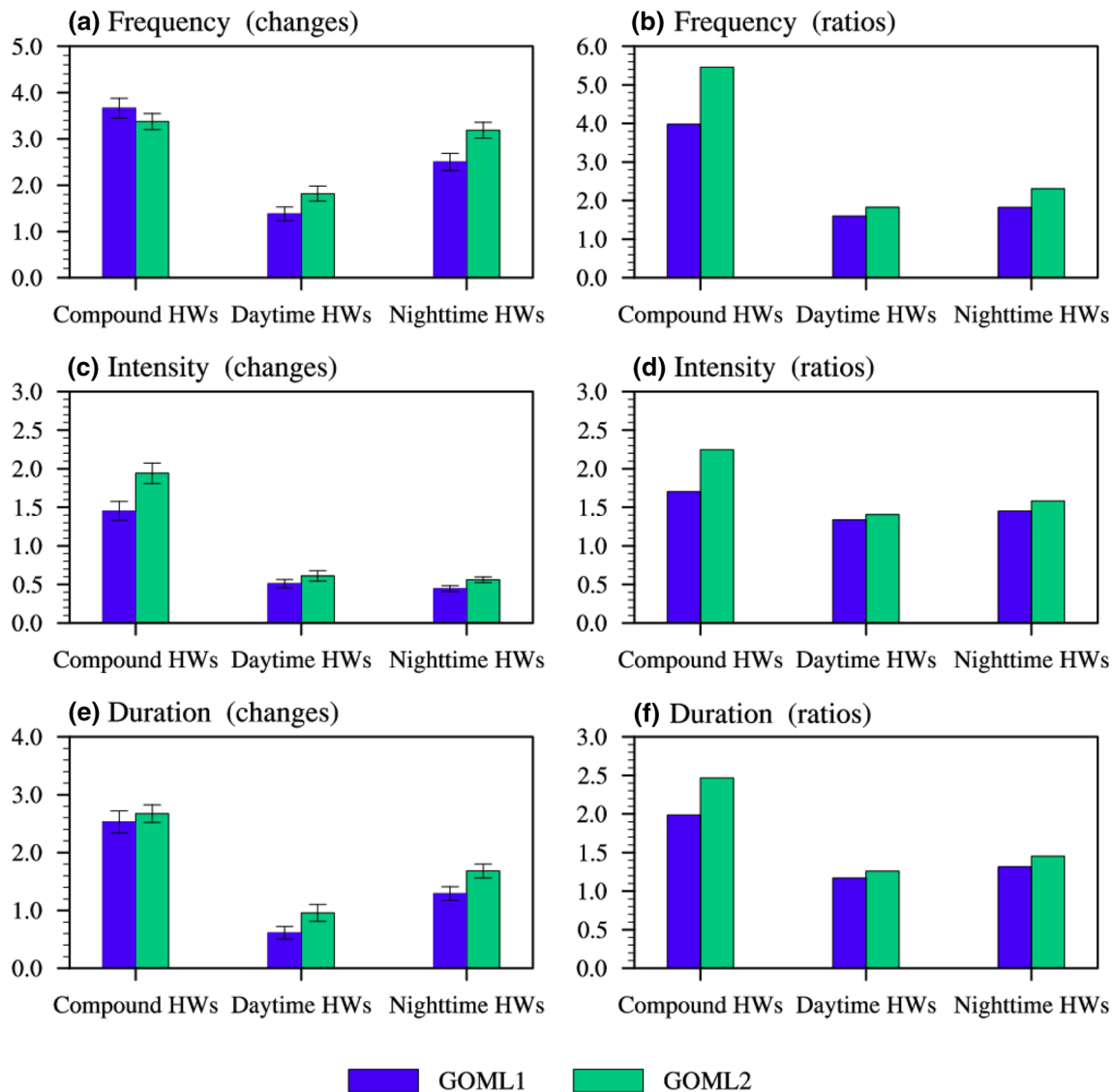


Fig. 6 Area averaged future changes of frequency (a), intensity (c), and duration (e) of compound, daytime, and nighttime HWs over whole China and the ratios of these three features in the FP projection to the PD (b, d, f) in MetUM-GOML1 and MetUM-GOML2. Units

these features for MetUM-GOML1 and MetUM-GOML2. The area-averaged future changes and ratios of three types of HWs over China in MetUM-GOML1 in most aspects agree with those in MetUM-GOML2.

For compound HWs, future changes in frequency and duration in the two models are similar, but the increase in intensity in MetUM-GOML1 is slightly less than that in MetUM-GOML2. The area-averaged future changes in frequency, intensity and duration of compound HWs over whole mainland China are 3.61 (3.37) events per year, 1.46 (1.94) °C/day and 2.50 (2.67) days in MetUM-GOML1 (MetUM-GOML2), respectively (Fig. 6a, c, e). Compared with the PD, the frequency of compound HWs in the FP

for frequency, intensity, and duration are events year⁻¹, °C day⁻¹, and days, respectively. The error bars indicate the 90% confidence intervals based on two-tailed Student's *t* test

increases remarkably, reaching 4–5 times the frequency in the PD, and the intensity and duration in the FP are roughly double (Fig. 6b, d, f).

For daytime HWs, the changes in frequency, intensity and duration over China in MetUM-GOML1 are very close to those in MetUM-GOML2, with values of 1.38 events per year, 0.51 °C/day and 0.61 days in MetUM-GOML1 relative to those ones of 1.82 events per year, 0.61 °C/day and 0.96 days in MetUM-GOML2 (Fig. 6a, c, e). Future changes of daytime HWs are significant but weaker than those of compound HWs. The frequency of daytime HWs in the FP increases by 60–80% relative to that in the PD,

the intensity increases by around 40%, and the duration increases by 20–30% (Fig. 6b, d, f).

For nighttime HWs, the changes in intensity over China are similar in two models, with value of 0.45 °C/day in MetUM-GOML1 and 0.58 °C/day in MetUM-GOML2 (Fig. 6c), while the changes in frequency and duration over China in MetUM-GOML1, with values of 2.50 events per year and 1.29 days, are about 3/4 of those in MetUM-GOML2, which are 3.19 events per year and 1.68 days (Fig. 6a, e). Future changes in nighttime HWs are slightly larger than those for daytime HWs, but weaker than those for compound HWs. The frequency of nighttime HWs in the FP almost doubles that in the PD, and the intensity and duration of nighttime HWs in the FP increase by 50–60% and 30–50% relative to those in the PD (Fig. 6b, d, f).

In order to get more clarity on what these projected future changes of three types of HWs exactly mean in context of past changes, the future changes in HWs over China are compared to the past decadal changes in HWs across the mid-1990s, which are indicated by the differences between PD and EP in observations (Su and Dong 2019). Nearly all projected future changes of the three types of HWs are stronger than the corresponding decadal changes across the mid-1990s. Specifically, the projected future changes in frequency of compound HWs relative to PD and all three aspects of daytime HWs are 2–4 times the decadal changes across the mid-1990s in observations. The future increase in the duration of compound HWs and frequency and duration of nighttime HWs are 20–80% larger than their decadal counterparts. These results suggest people will encounter much fiercer changes of HWs over China in the near future than they have experienced across the mid-1990s.

Summarizing the results above, all the compound, daytime, and nighttime HWs over China are projected to occur more frequently with strengthened intensity and elongated duration in the future. Quantitatively, the increases in all three aspects of compound HWs in the FP are the most remarkable with the frequency being 4–5 times that in the PD and the intensity and duration nearly doubling those in the PD. The increases in all three aspects of daytime and nighttime HWs are also considerable, with those of nighttime HWs larger than those of daytime HWs. The results of MetUM-GOML1 and MetUM-GOML2 are similar in terms of spatial patterns and area-averaged quantities of the future changes in the three types of HWs over China, suggesting these projected changes are robust at least for the two models used in this study.

4.3 Contributions of changes in mean state and variability to future changes of heat waves

Changes in HWs can arise from both a shift of the temperature distribution and changes in temperature variability, such

as a widening of the temperature distribution (Meehl and Tebaldi 2004; Schär et al. 2004; Lau and Nath 2014; Schoetter et al. 2015; Argueso et al. 2016; Guirguis et al. 2018). These studies suggested that both factors will contribute to HW changes in future and indicated an important role of temperature variability in shaping future HWs over North America and Europe. However, the role of a shift in the temperature distribution and change in temperature variability on future changes in HWs over China have not studied. So, the respective contributions of them to the future changes in HWs over China projected in the two models are assessed in this subsection.

Figure 7 illustrates the future changes in the extended summer mean surface air temperatures over China. T_{max} increases by more than 1.5 °C over most of China, with distinct areas of maximum increase over southern, northwestern and northeastern China (Fig. 7a, b). T_{min} increases more or less uniformly over most of China by more than 1.5 °C, but with relatively large increases over the northern margin of mainland China and relatively small increases over the southern margin of mainland China (Fig. 7c, d). All these main features of changes in T_{max} and T_{min} are similar in both models despite some slight differences. The increase centre of T_{max} over the southern China locates in southeastern China in MetUM-GOML1 but in central-southern China in MetUM-GOML2 (Fig. 7a, b). The increase in T_{min} over the southern and northern margins of mainland China is greater in MetUM-GOML2 than in MetUM-GOML1 (Fig. 7c, d). What should be mentioned, the spatial patterns of future changes in all three types of HWs are consistent with those of surface air temperatures. For example, the location of maximum increase in intensity and duration of compound and daytime HWs over southern China in both models (Figs. 3c–f, 4c–f) corresponds to the location of a substantial increase in T_{max} (Fig. 7a, b). The large increase in the intensity of compound and nighttime HWs over the northern margin of mainland China (Figs. 3c, d, 5c, d) corresponds to the large increase in T_{min} over the same region (Fig. 7c, d).

To obtain the mean temperature change induced and temperature variability change induced future changes of HWs separately, the HWs in the future related to the mean temperature changes are obtained based on constructed daily surface air temperatures (T_{max} and T_{min}) by adding the climatological differences in extended summer mean surface air temperatures between the C-FP and C-PD experiments (Fig. 7) to daily surface air temperatures in the C-PD experiments. Then the temperature variability change induced future changes of HWs are obtained by subtracting the mean temperature change induced future changes of HWs from the total future changes of HWs, which refer to the difference between the C-FP and C-PD experiments.

Figure 8 shows the total, mean temperature change induced, and temperature variability change induced future

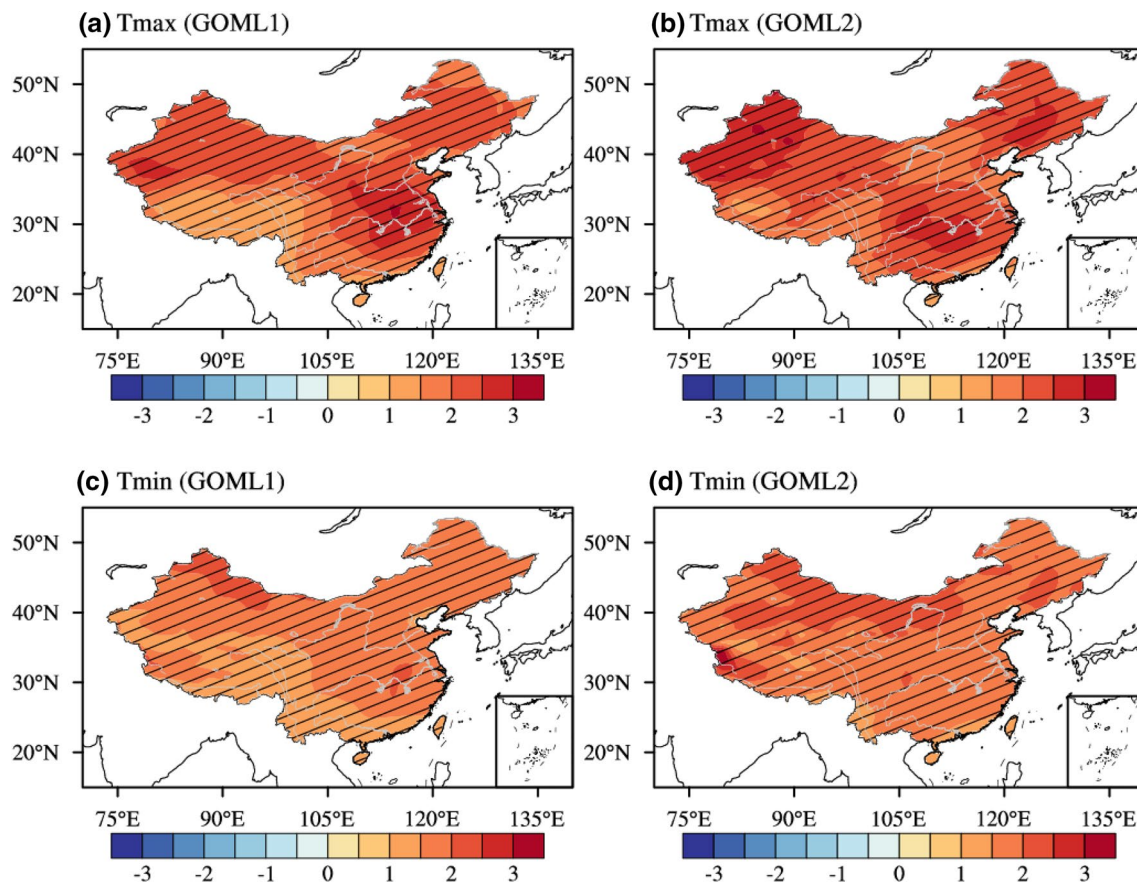


Fig. 7 Future changes in the extended-summer-mean (May–September) T_{\max} and T_{\min} relative to PD simulations in MetUM-GOML1 (**a**, **c**) and MetUM-GOML2 (**b**, **d**). Units are in $^{\circ}\text{C}$. The slashes highlight

the regions where the differences are statistically significant at the 90% confidence level based on a two-tailed Student's t test

changes of three types of HWs averaged over whole mainland China in MetUM-GOML1 and MetUM-GOML2. Future changes of HWs predominantly result from the mean temperature change, which accounts for more than 79% of total future change. The spatial patterns of various properties of the three types of HWs induced by a mean temperature change and a temperature variability change were also examined (not shown). The spatial patterns are consistent with the area-averaged results shown in Fig. 8. The spatial patterns of the mean temperature change induced future changes of HWs are quite similar to those of total future changes (Figs. 3, 4, 5) and the temperature variability change induced future changes of HWs are weak and only significant over small regions.

The results above indicate that changes in mean temperature play a predominant role in shaping future changes of HWs over China in MetUM-GOML1 and MetUM-GOML2. These results are in agreement with Argueso et al. (2016), who showed that seasonal mean temperature changes control future changes in HWs over large areas of the globe by using CMIP5 simulations. The subtle differences in future

changes of HWs between MetUM-GOML1 and MetUM-GOML2 also result from the slight differences in their projected future changes in the mean state. The physical processes responsible for the future changes in the mean surface air temperatures and subsequently the future changes of the three types of HWs are discussed in next section.

5 Physical processes responsible for simulated future changes of heat waves

The spatial patterns of future extended-summer-mean changes of some key variables in MetUM-GOML1 and MetUM-GOML2 are illustrated in Figs. 9 and 10. The main features of the changes in physical variables in the two models are similar. The most important features are increased surface downward longwave (LW) radiations everywhere (Fig. 9a, b), induced partly by the increase in GHG concentrations via the greenhouse effect and partly by the increase in water vapour in the atmosphere

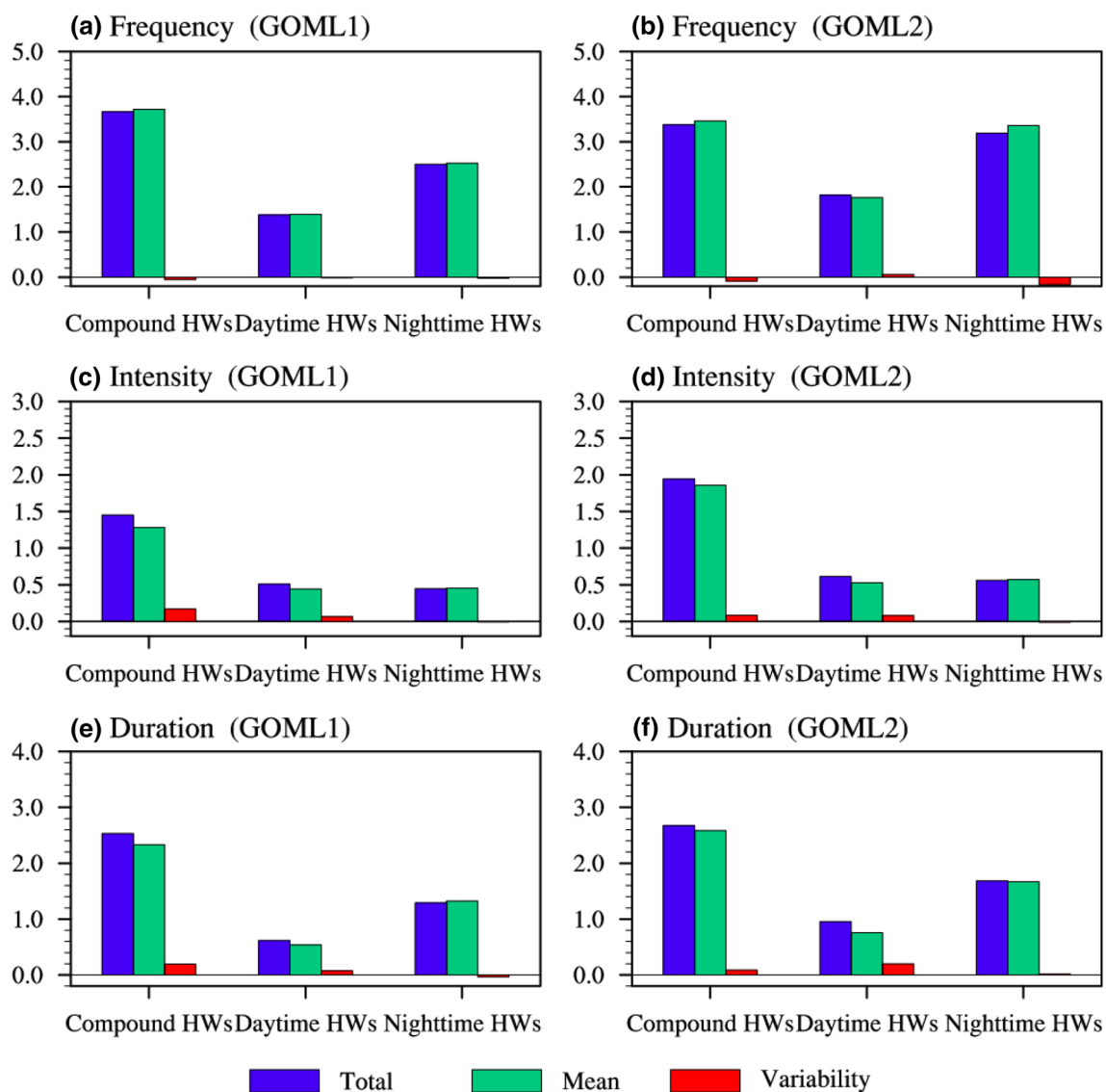


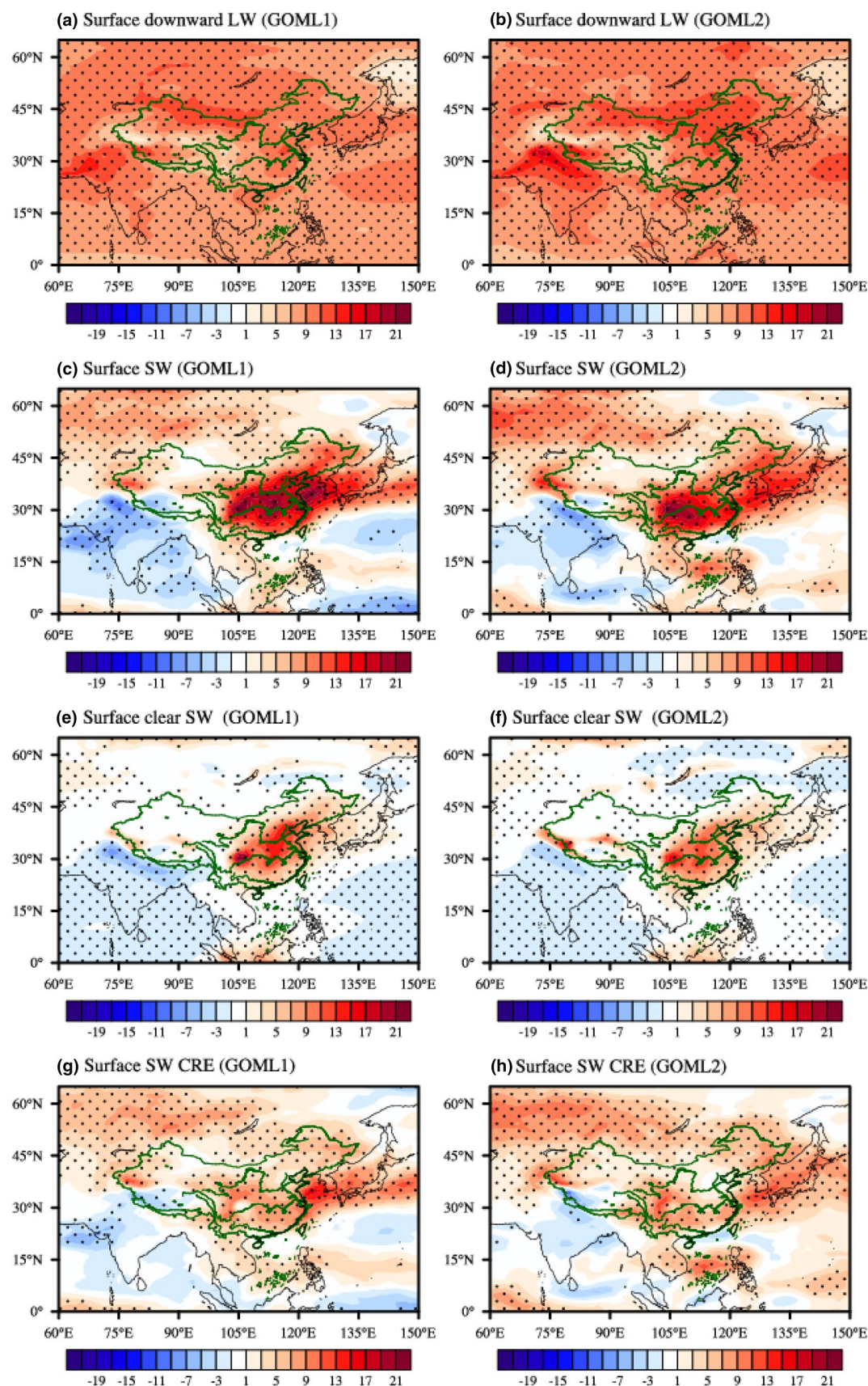
Fig. 8 Area averaged total, mean temperature change induced, temperature variability-change induced future changes in frequency (units: events year⁻¹; **a, b**), intensity (units: °C day⁻¹; **c, d**), and dura-

tion (units: days; **e, f**) of compound, daytime, and nighttime HWs over whole China in MetUM-GOML1 (left panels) and MetUM-GOML2 (right panels)

(Fig. 10a, b). The relatively large increase of downward LW radiation by about 7–9 W m⁻² over the eastern part of China is consistent with large increase of water vapour in the atmosphere by more than 3 kg m⁻², where the moisture transport from ocean to land is enhanced (not shown) due to strengthened East Asian Summer Monsoon (EASM) and more evaporation from ocean under the warming climate. Both the increased GHG concentrations and decreased AA emissions increase the land-sea thermal contrast by warming land more than ocean and enhance the EASM (not shown). This response of circulation is consistent with the previous studies (Lau and Kim 2017; Lau et al. 2017). The relatively large increase in surface downward LW radiation (9–11 W m⁻²) over the northern margin of China are

primarily due to the enhanced greenhouse effect (Fig. 9a, b) since the increase in water vapour in the atmosphere here is relatively small (Fig. 10a, b), and land surface and atmospheric feedbacks are weak due to the very dry underlying surface (Dong et al. 2009).

The changes of net surface shortwave (SW) radiation indicate an increase over most of China (Fig. 9c, d). This increase is contributed to by the increase in surface clear SW radiation over southeastern and northeastern China (Fig. 9e, f) and the positive anomalies of shortwave cloud radiative effect (SW CRE) over most of China (Fig. 9g, h). The increase in surface clear SW radiation over southeastern and northeastern China is induced by a reduction of total aerosol optical depth (AOD; Fig. 10c, d) through aerosol–radiation



◀Fig. 9 Spatial patterns of future extended-summer-mean changes in surface downward LW radiation (**a**, **b**), net surface SW radiation (**c**, **d**), surface clear SW radiation (**e**, **f**), and surface SW CRE (**g**, **h**) in MetUM-GOML1 (left panels) and MetUM-GOML2 (right panels). Radiation with positive value meaning downward and in W m^{-2} . The black dots highlight regions where the changes are statistically significant at the 90% confidence level based on a two-tailed Student's *t* test

interaction, which is primarily due to the decrease in sulphur dioxide emissions (Fig. 1).

The positive anomalies of SW CRE over most of China (Fig. 9g, h) result from a decrease in cloud cover over most of China (Fig. 10e, f) and the change of cloud radiative property due to the reduction of aerosol emissions over southeastern and northeastern China through cloud albedo effect of aerosol–cloud interaction (Twomey 1977). From the perspective of change of cloud radiative property, the decrease in aerosol emissions over southeastern and northeastern China leads to an increase in cloud droplet size (not shown) and a decrease in cloud droplet number concentration (not shown), resulting in a decrease in the reflectance of clouds and therefore positive anomalies of SW CRE relative to the high aerosol emissions during PD. From the perspective of decrease in cloud cover, different physical processes are responsible for the decrease in cloud cover over different sub-regions. Over northwestern China, the reduction of cloud cover is induced by a decrease in relative humidity (Fig. 10g, h), which under the global warming scenario is attributed to that water vapour in the atmosphere over land is controlled mainly by transport from the ocean and constrained by ocean warming and increases less than saturation specific humidity following the Clausius–Clapeyron relationship because of stronger warming over land than over the ocean (e.g., Dong et al. 2009; Boé and Terray 2014). Over southeastern China, the cloud cover decreases due to cloud lifetime effect of aerosol–cloud interaction (Albrecht 1989). Over northeastern China, the reduction of cloud cover is caused by both the decrease in relative humidity and the cloud lifetime effect of aerosol–cloud interaction.

In summary, the surface air temperature during extended summer over China in the mid-21st century is raised by the increase in surface downward LW radiation related to the enhanced greenhouse effect and the increased water vapour in the atmosphere over China, resulting from the enhanced EASM and increased evaporation from ocean, and by the increase in surface SW radiation related to the decreased cloud cover over most of China and the decreased AOD over southeastern and northeastern China. These physical processes responsible for the future increases in surface air temperature over China are almost the same in MetUM-GOML1 and MetGOML2. As a direct result of this overall warming, the frequency, intensity and duration of compound, daytime, and nighttime HWs over China are projected to increase in the future.

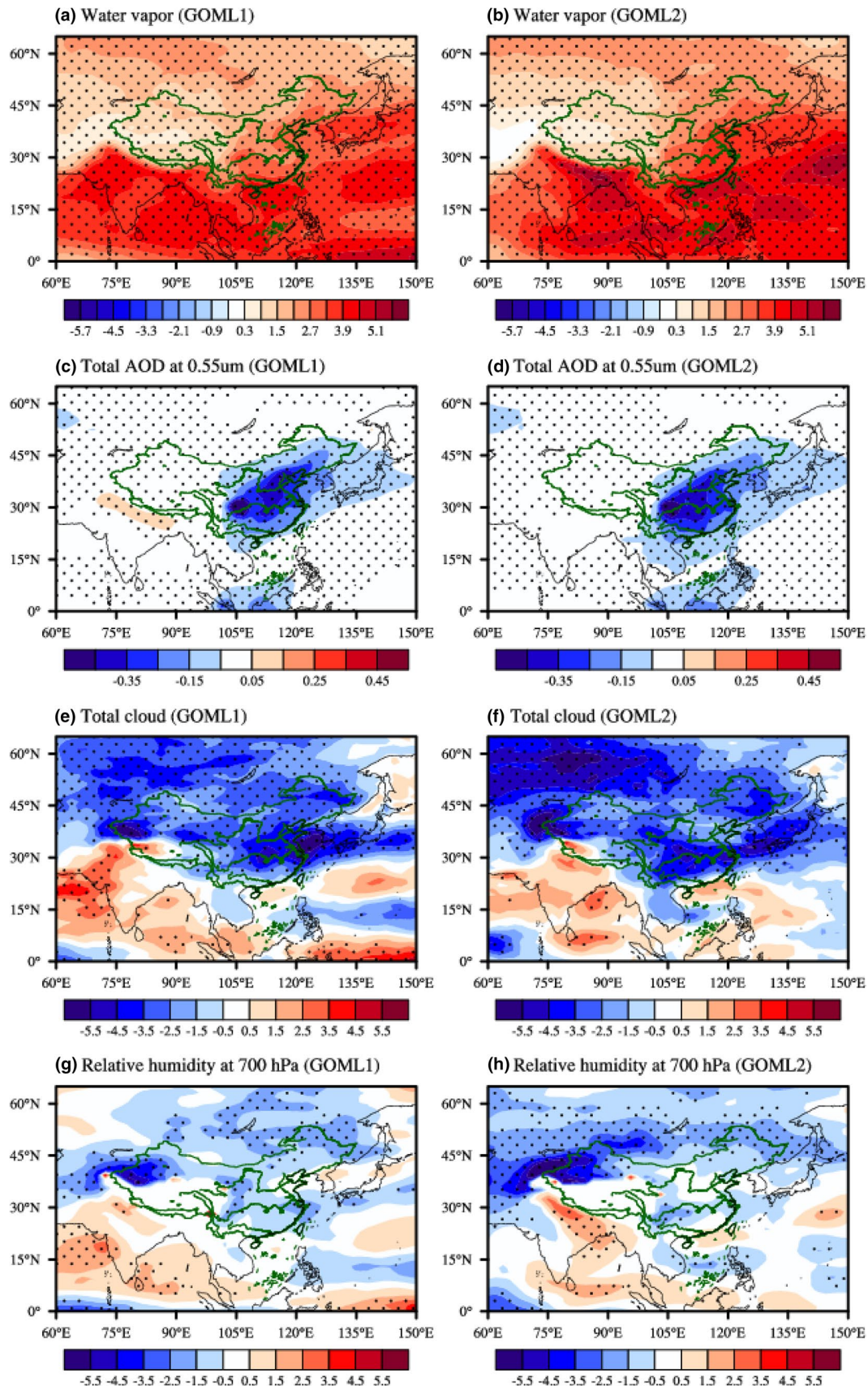
The slight difference in the change of seasonal mean surface air temperature between MetUM-GOML1 and MetUM-GOML2 is induced by the differences in the increase in surface SW radiation and the increase in surface downward LW radiation, which subsequently lead to the subtle differences in the future changes of three types of HWs. The surface SW radiation increases more over southeastern China in MetUM-GOML1 but over central-southern part of China in MetUM-GOML2 (Fig. 9b, c), leading to different locations of maximum T_{\max} change (Fig. 7a, b). The surface downward LW radiation increases more over the northern margin of mainland China and central-northern China in MetUM-GOML2 than in MetUM-GOML1 (Fig. 9a, b), resulting in a large increase in T_{\min} over these regions. These differences in surface SW radiation and downward LW radiation are attributed to the slight differences in atmospheric circulations between the two models, since the atmospheric circulations determine the aerosol distribution, water vapour transport and large-scale precipitation, which have direct or indirect effects on the energy budgets.

6 Conclusions

Future changes in the compound, daytime, and nighttime HWs over China during extended summer (May–September) in the mid-21st century (FP, 2045–2055) under RCP4.5 scenario relative to present day (PD, 1994–2011) are investigated in the aspects of frequency, intensity, and duration in this study. Numerical experiments performed by two coupled models, comprising the atmospheric components of two state-of-the-art climate models coupled to a multi-level mixed-layer ocean model and having much smaller sea surface temperature biases than fully coupled general circulation models, are used to evaluate the future changes in the HWs and to reveal the physical processes associated with these changes. The principal results are concluded below.

Compound, daytime and nighttime HWs over China are projected to be of more frequent occurrence with strengthened intensity and elongated duration under the scenario of increased GHG concentrations and decreased aerosol emissions over the Eurasian continent. The change in compound HWs will be the most dramatical in all three aspects, with the frequency in the FP being 4–5 times that in the PD, and the intensity and duration almost doubling those in the PD. The changes of daytime and nighttime HWs are also remarkable, with the increase of nighttime HWs being larger than those of daytime HWs. The projected future changes of HWs over China are determined mainly by changes in seasonal mean surface air temperatures (T_{\max} and T_{\min}), with changes in temperature variability playing a minor role.

Surface air temperatures over China are raised by increased downward LW radiation and increased surface SW



◀Fig. 10 Spatial patterns of future extended-summer-mean changes in column-integrated water vapour (**a**, **b**; units: kg m^{-2}), total AOD at 0.55 μm (**c**, **d**), total cloud cover (**e**, **f**; units: %), and relative humidity at 700 hPa (**g**, **h**; units: %) in MetUM-GOML1 (left panels) and MetUM-GOML2 (right panels). The black dots highlight regions where the changes are statistically significant at the 90% confidence level based on a two-tailed Student's *t* test

radiation, which therefore increases the frequency, intensity and duration of all three types of HWs. The increase in surface downward LW radiation is induced by the enhanced greenhouse effect and the increased water vapour in the atmosphere, resulting from the enhanced EASM and increased ocean evaporation in the warming climate. The increase in surface SW radiation is induced partly by the decreased cloud cover due to the reduced relative humidity in a warming world and partly by the decreased aerosol emissions via direct aerosol–radiation interaction and indirect aerosol–cloud interaction over southeastern and northeastern China.

The future changes of the three types of HWs over China in MetUM-GOML1 and MetUM-GOML2 are consistent in terms of spatial pattern and area averaged quantities. Although slight differences exist between two models, the projected increase in the frequency, intensity and duration of the three types of HWs over China under RCP4.5 scenario is robust among the two models used in this study.

Projected future changes of the three types of HWs over China in the mid-21st century relative to the present day are stronger than their decadal changes across the mid-1990s. Notably, projected future changes relative to PD in the frequency of compound HWs and all three aspects of daytime HWs are 2–4 times of the corresponding decadal changes across the mid-1990s in observations. The future increases in the duration of compound HWs and the frequency and duration of nighttime HWs are 20–80% larger than their decadal changes across the mid-1990s. These results suggest people will encounter much fiercer changes of HWs over China in the future than they have experienced across the mid-1990s and China would face a challenge to take adaptation measures to cope with the projected frequency increase, intensity enhancement and duration extension of HWs.

Future changes of HWs over China in the mid-21st century are projected under RCP4.5 scenario in this paper. Single RCP4.5 scenario is adopted in this study because the radiative forcings in the four scenarios of RCP2.6, RCP4.5, RCP6.0, and RCP8.5 are similar in the mid-21st century (Moss et al. 2010). However, in the further future, e.g., the end of 21st century, the projection under different scenarios should be concerned. In addition, there are some other factors influencing the HWs on the other timescales. For example, the variations of western North Pacific Subtropical High, East Asian Jet Stream, and El Niño-Southern Oscillation have an impact on the interannual variability of the

HWs over China (Wang et al. 2013, 2016; Luo and Lau 2017, 2018). These factors should be taken into consideration when forecasting the HWs on a shorter timescale.

Acknowledgements This study is supported by the National Natural Science Foundation of China under Grants 41505037 and 41875103, by the Applied Basic Research Foundation of Yunnan Province (2016FB078), and by the UK-China Research & Innovation Partnership Fund through the Met Office Climate Science for Service Partnership (CSSP) China as part of the Newton Fund. QS is supported by the China Scholarship Council. BD is supported by the U.K. National Centre for Atmospheric Science-Climate (NCAS-Climate) at the University of Reading. The authors like to thank three anonymous reviewers for their constructive comments on the earlier version of the paper.

References

- Albrecht BA (1989) Aerosols, cloud microphysics, and fractional cloudiness. *Science* 245(4923):1227–1230. <https://doi.org/10.1126/science.245.4923.1227>
- Argueso D, Di Luca A, Perkins-Kirkpatrick SE, Evans JP (2016) Seasonal mean temperature changes control future heat waves. *Geophys Res Lett* 43(14):7653–7660. <https://doi.org/10.1002/2016GL069408>
- Arribas A, Glover M, Maidens A, Peterson K, Gordon M, MacLachlan C, Graham R, Fereday D, Camp J, Scaife A (2011) The GloSea4 ensemble prediction system for seasonal forecasting. *Mon Weather Rev* 139(6):1891–1910. <https://doi.org/10.1175/2010MWR3615.1>
- Black E, Blackburn M, Harrison G, Hoskins B, Methven J (2004) Factors contributing to the summer 2003 European heatwave. *Weather* 59(8):217–223. <https://doi.org/10.1256/wea.74.04>
- Boé J, Terray L (2014) Land-sea contrast, soil-atmosphere and cloud-temperature interactions: interplays and roles in future summer European climate change. *Clim Dyn* 42(3–4):683–699. <https://doi.org/10.1007/s00382-013-1868-8>
- Chen W, Dong B (2018) Anthropogenic impacts on recent decadal change in temperature extremes over China: relative roles of greenhouse gases and anthropogenic aerosols. *Clim Dyn* 1:1. <https://doi.org/10.1007/s00382-018-4342-9>
- Chen Y, Li Y (2017) An inter-comparison of three heat wave types in China during 1961–2010: observed basic features and linear trends. *Sci Rep* 7:45619. <https://doi.org/10.1038/srep45619>
- Chen RD, Lu RY (2014) Large-scale circulation anomalies associated with ‘tropical night’ weather in Beijing, China. *Int J Climatol* 34(6):1980–1989. <https://doi.org/10.1002/joc.3815>
- Chen Y, Zhai P (2017) Revisiting summertime hot extremes in China during 1961–2015: overlooked compound extremes and significant changes. *Geophys Res Lett*. <https://doi.org/10.1002/2016GL072281>
- Chen Y, Chen W, Su Q, Luo F, Sparrow S, Tian F, Dong B, Tett SFB, Lott FC, Wallom D (2019) Anthropogenic warming has substantially increased the likelihood of July 2017-like heat waves over Central-Eastern China [in “Explaining Extremes of 2017 from a Climate Perspective”]. *Bull Amer Meteor Soc* 100(1):S91–S95. <https://doi.org/10.1175/BAMS-D-18-0087.1>
- Coumou D, Rahmstorf S (2012) A decade of weather extremes. *Nat Clim Change* 2(7):491–496. <https://doi.org/10.1038/nclimate1452>
- Della-Marta PM, Luterbacher J, von Weissenfluh H, Xoplaki E, Brunet M, Wanner H (2007) Summer heat waves over western Europe 1880–2003, their relationship to large-scale forcings and predictability. *Clim Dyn* 29(2):251–275. <https://doi.org/10.1007/s00382-007-0233-1>

- Dong B, Gregory JM, Sutton RT (2009) Understanding land–sea warming contrast in response to increasing greenhouse gases. Part I: Transient adjustment. *J Clim* 22(11):3079–3097. <https://doi.org/10.1175/2009JCLI2652.1>
- Dong B, Sutton RT, Shaffrey L, Klingaman NP (2017) Attribution of forced decadal climate change in coupled and uncoupled ocean–atmosphere model experiments. *J Clim* 30(16):6203–6223. <https://doi.org/10.1175/jcli-d-16-0578.1>
- Freychet N, Tett S, Wang J, Hegerl G (2017) Summer heat waves over Eastern China: dynamical processes and trend attribution. *Environ Res Lett* 12(2):024015. <https://doi.org/10.1088/1748-9326/aa5ba3>
- Freychet N, Sparrow S, Tett SFB, Mineter MJ, Hegerl GC, Wallom DCH (2018) Impacts of anthropogenic forcings and El Niño on Chinese extreme temperatures. *Adv Atmos Sci* 35(8):994–1002. <https://doi.org/10.1007/s00376-018-7258-8>
- Gershunov A, Cayan DR, Iacobellis SF (2009) The great 2006 heat wave over California and Nevada: signal of an increasing trend. *J Clim* 22(23):6181–6203. <https://doi.org/10.1175/2009JCLI2465.1>
- Gosling SN, Lowe JA, McGregor GR, Pelling M, Malamud BD (2009) Associations between elevated atmospheric temperature and human mortality: a critical review of the literature. *Clim Change* 92(3–4):299–341. <https://doi.org/10.1007/s10584-008-9441-x>
- Guirguis K, Gershunov A, Cayan DR, Pierce DW (2018) Heat wave probability in the changing climate of the Southwest US. *Clim Dyn* 50(9–10):3853–3864. <https://doi.org/10.1007/s00382-017-3850-3>
- Guo X, Huang J, Luo Y, Zhao Z, Xu Y (2017) Projection of heat waves over China for eight different global warming targets using 12 CMIP5 models. *Theor Appl Climatol* 128(3–4):507–522. <https://doi.org/10.1007/s00704-015-1718-1>
- Hatfield JL, Prueger JH (2015) Temperature extremes: effect on plant growth and development. *Weather Clim Extremes* 10:4–10. <https://doi.org/10.1016/j.wace.2015.08.001>
- Hirons L, Klingaman N, Woolnough S (2015) MetUM-GOML: a near-globally coupled atmosphere–ocean-mixed-layer model. *Geosci Model Dev* 8:363–379. <https://doi.org/10.5194/gmd-8-363-2015>
- Jones C et al (2011) The HadGEM2-ES implementation of CMIP5 centennial simulations. *Geosci Model Dev* 4(3):543–570. <https://doi.org/10.5194/gmd-4-543-2011>
- Karl TR, Knight RW (1997) The 1995 Chicago heat wave: how likely is a recurrence? *Bull Am Meteor Soc* 78(6):1107–1120. [https://doi.org/10.1175/1520-0477\(1997\)078%3c1107:tchwhl%3e2.0.co;2](https://doi.org/10.1175/1520-0477(1997)078%3c1107:tchwhl%3e2.0.co;2)
- Lamarque J-F, Bond TC, Eyring V, Granier C, Heil A, Klimont Z, Lee D, Lioussse C, Mieville A, Owen B (2010) Historical (1850–2000) gridded anthropogenic and biomass burning emissions of reactive gases and aerosols: methodology and application. *Atmos Chem Phys* 10(15):7017–7039. <https://doi.org/10.5194/acp-10-7017-2010>
- Lamarque J-F, Kyle GP, Meinshausen M, Riahi K, Smith SJ, van Vuuren DP, Conley AJ, Vitt F (2011) Global and regional evolution of short-lived radiatively-active gases and aerosols in the representative concentration pathways. *Clim Change* 109:191. <https://doi.org/10.1007/s10584-011-0155-0>
- Lau WKM, Kim KM (2017) Competing influences of greenhouse warming and aerosols on Asian summer monsoon circulation and rainfall. *Asia-Pac J Atmos Sci* 53(2):181–194. <https://doi.org/10.1007/s13143-017-0033-4>
- Lau N-C, Nath MJ (2014) Model simulation and projection of European heat waves in present-day and future climates. *J Clim* 27(10):3713–3730. <https://doi.org/10.1175/jcli-d-13-00284.1>
- Lau WKM, Kim KM, Leung LR (2017) Changing circulation structure and precipitation characteristics in Asian monsoon regions: greenhouse warming vs. aerosol effects. *Geosci Lett* 4(1):28. <https://doi.org/10.1186/s40562-017-0094-3>
- Lesk C, Rowhani P, Ramankutty N (2016) Influence of extreme weather disasters on global crop production. *Nature* 529(7584):84. <https://doi.org/10.1038/nature16467>
- Li Z, Cao LJ, Zhu YN, Yan ZW (2016) Comparison of two homogenized datasets of daily maximum/mean/minimum temperature in China during 1960–2013. *J Meteor Res* 30(1):53–66. <https://doi.org/10.1007/s13351-016-5054-x>
- Li Y, Ding Y, Li W (2017) Observed trends in various aspects of compound heat waves across China from 1961 to 2015. *J Meteor Res* 31(3):455–467. <https://doi.org/10.1007/s13351-017-6150-2>
- Luo M, Lau N-C (2017) Heat waves in southern China: synoptic behavior, long-term change, and urbanization effects. *J Clim* 30(2):703–720. <https://doi.org/10.1175/jcli-d-16-0269.1>
- Luo M, Lau N-C (2018) Synoptic characteristics, atmospheric controls, and long-term changes of heat waves over the Indo-China Peninsula. *Clim Dyn* 51(7–8):2707–2723. <https://doi.org/10.1007/s00382-017-4038-6>
- Luo F, Dong B, Tian F, Li S (2018) Anthropogenically forced decadal change of South Asian summer monsoon across the mid-1990s. *J Geophys Res Atmos* 124(2):806–824. <https://doi.org/10.1029/2018jd029195>
- Ma SM, Zhou TJ, Stone DA, Angelil O, Shiogama H (2017) Attribution of the July–August 2013 heat event in Central and Eastern China to anthropogenic greenhouse gas emissions. *Environ Res Lett*. <https://doi.org/10.1088/1748-9326/aa69d2>
- Meehl GA, Tebaldi C (2004) More intense, more frequent, and longer lasting heat waves in the 21st Century. *Science* 305(5686):994–997. <https://doi.org/10.1126/science.1098704>
- Moss RH, Edmonds JA, Hibbard KA, Manning MR, Rose SK, Vuuren DP, Van TR, Carter E, Seita K Mikiko, Tom K (2010) The next generation of scenarios for climate change research and assessment. *Nature* 463(7282):747–756. <https://doi.org/10.1038/nature08823>
- Perkins SE (2015) A review on the scientific understanding of heat-waves—their measurement, driving mechanisms, and changes at the global scale. *Atmos Res* 164–165:242–267. <https://doi.org/10.1016/j.atmosres.2015.05.014>
- Perkins SE, Alexander LV (2013) On the measurement of heat waves. *J Clim* 26(13):4500–4517. <https://doi.org/10.1175/jcli-d-12-0038.1>
- Rayner NA, Parker DE, Horton EB, Folland CK, Alexander LV, Rowell DP, Kent EC, Kaplan A (2003) Global analyses of SST, sea ice and night marine air temperature since the late nineteenth century. *J Geophys Res.* <https://doi.org/10.1029/2002JD002670>
- Robine JM, Cheung SLK, Le Roy S, Van Oyen H, Griffiths C, Michel JP, Herrmann FR (2008) Death toll exceeded 70,000 in Europe during the summer of 2003. *C R Biol* 331(2):171–178. <https://doi.org/10.1016/j.crvi.2007.12.001>
- Schär C, Vidale PL, Lüthi D, Frei C, Häberli C, Liniger MA, Appenzeller C (2004) The role of increasing temperature variability in European summer heatwaves. *Nature* 427(6972):332–336. <https://doi.org/10.1038/nature02300>
- Schoetter R, Cattiaux J, Douville H (2015) Changes of western European heat wave characteristics projected by the CMIP5 ensemble. *Clim Dyn* 45(5–6):1601–1616. <https://doi.org/10.1007/s00382-014-2434-8>
- Seneviratne SI, Donat MG, Mueller B, Alexander LV (2014) No pause in the increase of hot temperature extremes. *Nat Clim Change* 4(3):161. <https://doi.org/10.1038/nclimate2145>
- Smith DM, Murphy JM (2007) An objective ocean temperature and salinity analysis using covariances from a global climate model. *J Geophys Res Oceans*. <https://doi.org/10.1029/2005JC003172>
- Sparrow S, Su Q, Tian FX, Li SH, Chen Y, Chen W, Luo FF, Freychet N, Lott FC, Dong BW, Tett SFB, Wallom D (2018) Attributing human influence on the July 2017 Chinese heatwave: the

- influence of sea-surface temperatures. *Environ Res Lett.* <https://doi.org/10.1088/1748-9326/ade356>
- Stefanon M, Fabio DA, Philippe D (2012) Heatwave classification over Europe and the Mediterranean region. *Environ Res Lett* 7(1):014023. <https://doi.org/10.1088/1748-9326/7/1/014023>
- Su Q, Dong B (2019) Recent decadal changes in heat waves over China: drivers and mechanisms. *J Clim*
- Sun Y, Zhang XB, Zwiers FW, Song LC, Wan H, Hu T, Yin H, Ren GY (2014) Rapid increase in the risk to extreme summer heat in Eastern China. *Nat Clim Change* 4(12):1082–1085. <https://doi.org/10.1038/nclimate2410>
- Sun Y, Song L, Yin H, Zhou B, Hu T, Zhang X, Stott P (2016) Human influence on the 2015 extreme high temperature events in Western China [in “Explaining Extremes of 2015 from a Climate Perspective”]. *Bull Am Meteor Soc* 97(12):S102–S106. <https://doi.org/10.1175/bams-d-16-0158.1>
- Tan J, Zheng Y, Song G, Kalkstein LS, Kalkstein AJ, Tang X (2007) Heat wave impacts on mortality in Shanghai, 1998 and 2003. *Int J Biometeorol* 51(3):193–200. <https://doi.org/10.1007/s00484-006-0058-3>
- Tian F, Dong B, Robson J, Sutton R (2018) Forced decadal changes in the East Asian summer monsoon: the roles of greenhouse gases and anthropogenic aerosols. *Clim Dyn* 1:1–17. <https://doi.org/10.1007/s00382-018-4105-7>
- Twomey S (1977) Influence of pollution on shortwave albedo of clouds. *J Atmos Sci* 34(7):1149–1152. [https://doi.org/10.1175/1520-0469\(1977\)034%3c1149:tiopot%3e2.0.co;2](https://doi.org/10.1175/1520-0469(1977)034%3c1149:tiopot%3e2.0.co;2)
- Walters D, Best M, Bushell A, Copsey D, Copsey D, Edwards J, Falloon P, Harris C, Lock A, Manners J, Morcrette C (2011) The Met Office Unified Model global atmosphere 3.0/3.1 and JULES global land 3.0/3.1 configurations. *Geosci Model Dev* 4(4):919. <https://doi.org/10.5194/gmd-4-919-2011>
- Walters D, Wood N, Vosper S, Milton S (2014) ENDGame: a new dynamical core for seamless atmospheric prediction. Met Office documentation. <http://www.metoffice.gov.uk/media/pdf/s/h/ENDGameGOVSciv2.0.pdf>
- Walters D, Brooks M, Boutle I, Melvin T, Stratton R, Vosper S, Wells H, Williams K, Wood N, Allen T (2017) The Met Office unified model global atmosphere 6.0/6.1 and JULES global land 6.0/6.1 configurations. *Geosci Model Dev* 10(4):1487–1520. <https://doi.org/10.5194/gmd-10-1487-2017>
- Wang W, Zhou W, Wang X, Fong SK, Leong KC (2013) Summer high temperature extremes in Southeast China associated with the East Asian jet stream and circumglobal teleconnection. *J Geophys Res Atmos* 118(15):8306–8319. <https://doi.org/10.1002/jgrd.50633>
- Wang C, Zhang L, Lee S-K, Wu L, Mechoso CR (2014) A global perspective on CMIP5 climate model biases. *Nat Clim Change* 4:201–205. <https://doi.org/10.1038/nclimate2118>
- Wang W, Zhou W, Li X, Wang X, Wang D (2016) Synoptic-scale characteristics and atmospheric controls of summer heat waves in China. *Clim Dyn* 46(9):2923–2941. <https://doi.org/10.1007/s00382-015-2741-8>
- Wang P, Tang J, Sun X, Wang S, Wu J, Dong X, Fang J (2017) Heatwaves in China: definitions, leading patterns and connections to large-scale atmospheric circulation and SSTs. *J Geophys Res Atmos*. <https://doi.org/10.1002/2017JD027180>
- Wilbanks TJ, Fernandez S (2014) Climate change and infrastructure, urban systems, and vulnerabilities: technical report for the US department of energy in support of the national climate assessment. Island Press, Washington
- Wilcox LJ, Dong B, Sutton RT, Highwood EJ (2015) The 2014 hot, dry summer in Northeast Asia [in “Explaining Extremes of 2014 from a Climate Perspective”]. *Bull Am Meteor Soc* 96(12):S105–S110. <https://doi.org/10.1175/bams-d-15-00123.1>
- Xu Y, Ramanathan V, Victor DG (2018) Global warming will happen faster than we think. *Nature* 564:30–32. <https://doi.org/10.1038/d41586-018-07586-5>
- You QL, Jiang ZH, Kong L, Wu ZW, Bao YT, Kang SC, Pepin N (2017) A comparison of heat wave climatologies and trends in China based on multiple definitions. *Clim Dyn* 48(11):3975–3989. <https://doi.org/10.1007/s00382-016-3315-0>
- Yu R, Zhai PM, Lu YY (2018) Implications of differential effects between 1.5 and 2 °C global warming on temperature and precipitation extremes in China’s urban agglomerations. *Int J Climatol* 38(5):2374–2385. <https://doi.org/10.1002/joc.5340>
- Zhou B, Wen QH, Xu Y, Song L, Zhang X (2014a) Projected changes in temperature and precipitation extremes in China by the CMIP5 multimodel ensembles. *J Clim* 27(17):6591–6611. <https://doi.org/10.1175/jcli-d-13-00761.1>
- Zhou TJ, Ma SM, Zou LW (2014b) Understanding a hot summer in Central Eastern China: summer 2013 in context of multimodel trend analysis [in “Explaining Extremes of 2013 from a Climate Perspective”]. *Bull Am Meteor Soc* 95(9):S54–S57

Publisher's Note Springer Nature remains neutral with regard to jurisdictional claims in published maps and institutional affiliations.